

# High Surface Area SOFC Electrode Materials Prepared at Traditional Sintering Temperatures

S. P. Muhoza,<sup>1,\*</sup> T. E. Barrett,<sup>1</sup> M. A. Cottam,<sup>1</sup> S. E. Soll,<sup>1</sup> M. D. Yuce,<sup>1</sup> V. S. Prathab,<sup>1</sup> S. K. Hambright,<sup>1</sup> M. Rezazad,<sup>1</sup> O. Racchi,<sup>1</sup> and M. D. Gross<sup>2,3,z</sup>

Solid oxide fuel cell (SOFC) electrode materials with surface areas up to  $99 \text{ m}^2 \cdot \text{g}^{-1}$  were prepared at traditional sintering temperatures,  $1050^{\circ}\text{C}-1350^{\circ}\text{C}$ , by sintering hybrid inorganic-organic materials in an inert atmosphere followed by calcination in air at  $700^{\circ}\text{C}$ . The electrode materials investigated were yttria-stabilized zirconia (YSZ), lanthanum strontium cobalt ferrite (LSCF), gadolinia doped ceria (GDC), and strontium titanate (STO). During sintering, an amorphous carbon template forms in situ and remains throughout the sintering process, aiding in the creation and preservation of mixed-metal-oxide nanomorphology. The carbon template is removed during subsequent calcination in air at  $700^{\circ}\text{C}$ , leaving behind a nanostructured ceramic. Phase stability, carbon template concentration, and specific surface area was determined for each mixed-metal-oxide. Final specific surface area up to 83, 66, 95, and  $99 \text{ m}^2 \cdot \text{g}^{-1}$  were achieved for YSZ, LSCF, GDC, and STO, respectively. The impact of high surface area YSZ on symmetrical YSZ-lanthanum strontium ferrite (LSF) cathode cell performance was evaluated in the temperature range of  $550^{\circ}\text{C}-800^{\circ}\text{C}$ . Adding nanostructured YSZ decreased the electrochemical impedance by 45% at  $550^{\circ}\text{C}$ . The performance improvement lessened with increasing temperature, and at  $800^{\circ}\text{C}$  there was essentially no improvement. The findings reveal a promising approach to improving low temperature SOFC performance.

© 2018 The Electrochemical Society. [DOI: 10.1149/2.0381802jes]

Manuscript submitted November 30, 2017; revised manuscript received December 21, 2017. Published January 11, 2018.

Lowering the operating temperature of solid oxide fuel cells (SOFCs) has the potential to minimize materials cost and degradation rates, two of the main challenges facing successful SOFC commercialization. Moreover, low temperature-SOFCs (LT-SOFCs) broaden the portfolio of practical applications to portable, transportation, and energy storage in addition to the traditional stationary power generation applications. However, one major hurdle to overcome is the slow electrode kinetics at low temperatures, which increases electrochemical activation losses and impedes power output. 3-8

One approach to resolving poor LT-SOFC performance is to increase the density of electrochemically active sites in the electrode. Many research groups have focused on increasing the density of active sites by decorating the surface of pre-sintered scaffolds with electrocatalytic particles, 9-24 however little effort has been made to increase the surface area of the sintered scaffold itself. The surface area of electrocatalytic particles coating the scaffold has been shown to decrease with time until it approaches the scaffold surface area, and a concomitant decrease in performance was observed. Ultimately, the scaffold surface area dictated performance. Thus, it is important to consider strategies for increasing scaffold surface area.

The in situ carbon templating method reported in this work has great potential to increase the scaffold surface area and the density of electrochemically active sites for two reasons. First, SOFC electrode materials with surface areas up to  $99~\text{m}^2\cdot\text{g}^{-1}$  and  $69~\text{m}^2\cdot\text{g}^{-1}$  can be realized at sintering temperatures of  $1050^{\circ}\text{C}$  and  $1350^{\circ}\text{C}$ , respectively. The exceptionally high surface area,  $\sim \! 100$  times higher than traditionally sintered electrode materials,  $^{25-35}$  affords the opportunity to create a much higher density of electrochemically active sites.  $^{36,37}$  Second, the in situ carbon templating method is robust; here we show it works for two different types of hybrid inorganic-organic materials and four different SOFC electrode materials: yttriastabilized zirconia (YSZ, 8 mol%  $Y_2O_3$ ), lanthanum strontium cobalt ferrite (LSCF, La $_{0.6}Sr_{0.4}Co_{0.2}Fe_{0.8}O_{3.8}$ ), gadolinia doped ceria (GDC,  $Ce_{0.8}Gd_{0.2}O_{2.8}$ ), and strontium titanate (STO, SrTiO $_3$ ). Thus, it is likely that the method can be broadly applied to many hybrid materials and mixed-metal-oxides.

The in situ carbon templating method differs from the traditional sintering method in two fundamental ways as shown in Figure 1. First, metal oxide particles are physically mixed with pore formers in the traditional method, while hybrid inorganic-organic materials are used in

the carbon templating method. Second, materials are directly sintered in air in traditional sintering, whereas materials are sintered in argon and subsequently calcined in air in the carbon templating method. In the in situ carbon templating method, the organic component is pyrolyzed during sintering and leaves behind a carbon template which remains throughout the entire process. This carbon template prevents the metal oxides from coarsening during sintering and is removed upon calcination in air at 700°C, a temperature too low for significant sintering to occur.

In this paper we report on the following facets of the in situ carbon templating method using two types of hybrid inorganic-organic materials: (1) the phase stability of YSZ, LSCF, GDC, and STO as a function of sintering temperature, (2) the concentration of amorphous carbon template formed in situ as a function of hybrid material formulation, and (3) the impact of sintering temperature and hybrid material formulation on the specific surface area of each mixed-metal-oxide. Finally, as a proof-of-concept, improvement in the electrochemical performance of a YSZ-lanthanum strontium ferrite (LSF) cathode was observed when high surface area YSZ, generated by the in situ carbon templating method, was incorporated into the electrode.

### **Experimental**

Table I summarizes the experimental synthesis of all hybrid inorganic-organic materials prepared in this study. The two types of hybrid materials prepared are referred to as propylene oxide (PO) and citric acid (CA) hybrid materials. For all PO hybrid materials, the PO to total metals molar ratio (PO:M) was held constant at 10:1 and the glucose to total metals molar ratios (Glucose:M) were varied between 0:1, 2.5:1, and 5.0:1. As shown in Table I, the time for PO hybrid material formation spanned 5 minutes to 36 hours, depending on the mixed-metal-oxide. This large variation in time is consistent with the work of Gash et al., which found that the rate of PO hybrid material formation depends on the rate of hydrolysis and condensation, and these rates are strongly affected by the metal ion charge and electronic configuration. <sup>38,39</sup> All citric acid (CA) formulations are identified as a molar ratio of CA:ethylene glycol (EG):total metals (M). The CA:EG:M molar ratios were varied between 1:1:1, 5:5:1, and 10:10:1. The rate of CA hybrid material formation primarily depends on CA and EG polymerization<sup>40</sup> and, for this reason, roughly similar time scales were needed for all CA hybrid materials to form as shown in Table I.

<sup>&</sup>lt;sup>1</sup>Department of Chemistry, Wake Forest University, Winston-Salem, North Carolina 27109, USA

<sup>&</sup>lt;sup>2</sup>Department of Engineering, Wake Forest University, Winston-Salem, North Carolina 27101, USA

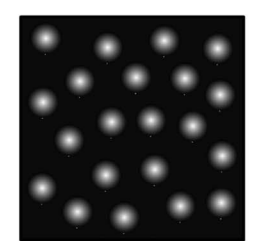
<sup>&</sup>lt;sup>3</sup>Center for Functional Materials, Wake Forest University, Winston-Salem, North Carolina 27109, USA

<sup>\*</sup>Electrochemical Society Student Member.

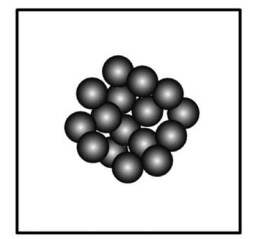
<sup>&</sup>lt;sup>z</sup>E-mail: grossmd@wfu.edu

# Traditional Sintering Approach

1) Physically Mix Metal Oxide Particles + Pore Formers



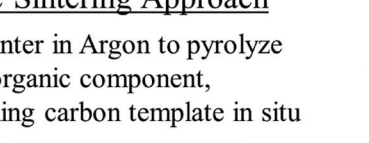
# 2) Sinter in Air



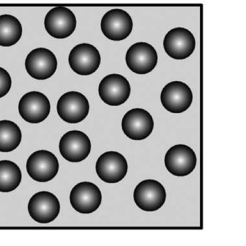
# In-Situ Carbon Template Sintering Approach

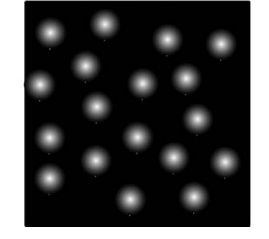
1) Hybrid Material organic matrix

2) Sinter in Argon to pyrolyze suspends metal ions in the organic component, forming carbon template in situ



3) Calcine in Air at low temperature to remove carbon template





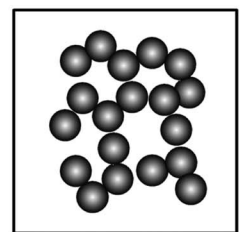


Figure 1. Schematic representation comparing traditional and in situ carbon templating sintering approaches.

PO hybrid materials of YSZ (YSZ-PO) were synthesized with ZrCl<sub>4</sub> (99.5+%, Alfa Aesar), Y(NO<sub>3</sub>)<sub>3</sub> · 6H<sub>2</sub>O (99.9%, Alfa Aesar), glucose (> 99.9%, Alfa Aesar), and PO (> 99.5%, Sigma-Aldrich) as described in detail elsewhere. 41–43 The salts were dissolved in deionized water in a Zr:Y:H<sub>2</sub>O molar ratio of 5.75:1:650 with magnetic stirring. Glucose was then dissolved in the solution and PO was subsequently added to the solution. Magnetic stirring was maintained until the hybrid material formed, typically within 5 minutes.

PO hybrid materials of LSCF (LSCF-PO) were similarly prepared except that a higher temperature was required for the hybrid materials to form. The hybrid materials were prepared with La(NO<sub>3</sub>)<sub>3</sub>·6H<sub>2</sub>O (99.99%, Alfa Aesar), Sr(NO<sub>3</sub>)<sub>2</sub> (99.0%, Alfa Aesar), Co(NO<sub>3</sub>)<sub>2</sub>·6H<sub>2</sub>O (Assay Percent Range 98.0%-102.0%, Alfa Aesar), Fe(NO<sub>3</sub>)<sub>3</sub> · 9H<sub>2</sub>O (98+%, Alfa Aesar), glucose, and PO. The salts were dissolved in deionized water in a La:Sr:Co:Fe:H<sub>2</sub>O molar ratio of 3:2:1:4:950. While magnetically stirring the solution, glucose was dissolved and then PO was added. The solution was then heated to 120°C until the hybrid materials formed, which in some cases took up to 12 hours.

PO hybrid materials of GDC (GDC-PO) were synthesized in a mixture of deionized water and ethanol (200 Proof, Decon Labs) with CeCl<sub>3</sub>·7H<sub>2</sub>O (99%, Alfa Aesar), GdCl<sub>3</sub>·6H<sub>2</sub>O (99%, Sigma-Aldrich), glucose, and PO. The salts were dissolved in a mixture of deionized water and ethanol (EtOH) in a Ce:Gd:H2O:EtOH molar ratio of 4:1:475:475. Glucose was then dissolved in the solution and magnetically stirred. PO was then added to the solution and the temperature was increased to 95°C until the hybrid materials formed, which took up to 36 hours in some instances.

The CA hybrid materials of YSZ, LSCF, and GDC are referred to as YSZ-CA, LSCF-CA, and GDC-CA. YSZ-CA was prepared with ZrCl<sub>4</sub> and YCl<sub>3</sub> (99.9%, Alfa Aesar). The salts were dissolved in deionized water in a Zr:Y:H<sub>2</sub>O molar ratio of 5.75:1:1150. LSCF-CA was prepared with La( $NO_3$ )<sub>3</sub> ·  $6H_2O$ , Sr( $NO_3$ )<sub>2</sub>, Co( $NO_3$ )<sub>2</sub> ·  $6H_2O$ , and Fe(NO<sub>3</sub>)<sub>3</sub> · 9H<sub>2</sub>O. The salts were dissolved in deionized water in a La:Sr:Co:Fe:H<sub>2</sub>O molar ratio of 3:2:1:4:1800. GDC-CA was prepared with CeCl<sub>3</sub> · 7H<sub>2</sub>O and GdCl<sub>3</sub> · 6H<sub>2</sub>O. Both salts were dissolved in deionized water in a Ce:Gd:H<sub>2</sub>O molar ratio of 4:1:850. In all three cases, CA (99.8%, USBiological) and EG (99.75%, Acros Organics)

were subsequently added to the solutions and magnetically stirred until complete dissolution. Then, the solutions were heated to 80°C for YSZ-CA and GDC-CA and 120°C for LSCF-CA. All solutions were magnetically stirred until the hybrid materials formed, typically within 6 hours.

The CA hybrid materials of STO are referred to as STO-CA and were prepared with TiCl<sub>3</sub> solution (≥ 12%, Sigma-Aldrich) and SrCl<sub>2</sub> · 6H<sub>2</sub>O (99+%, Alfa Aesar) in a 1:1 Sr:Ti molar ratio. Stoichiometric amounts of TiCl<sub>3</sub>, CA, and EG were mixed, heated to 60°C, and vigorously stirred until a homogeneous mixture was formed, typically within 10 minutes. SrCl<sub>2</sub> was then added to the solution and the temperature was raised to 80°C. Magnetic stirring was maintained until the hybrid material formed, typically within 6 hours.

All hybrid materials were sintered in a tube furnace under argon (99.998%, Airgas, Radnor, PA) flowing at 750 mL⋅min<sup>-1</sup>. The temperature was increased from ambient temperature to 850°C at 5°C·min<sup>-1</sup>, then from 850°C to the sintering temperature at  $2^{\circ}\text{C} \cdot \text{min}^{-1}$ , and held at the sintering temperature for 2 h. The temperature was then decreased from the sintering temperature to 850°C and ambient temperature at  $2^{\circ}\text{C} \cdot \text{min}^{-1}$  and  $5^{\circ}\text{C} \cdot \text{min}^{-1}$ , respectively. All hybrid material formulations were sintered at 1050°C, but PO hybrid materials with a 5:1 Glucose:M molar ratio and CA hybrid materials with a 10:10:1 CA:EG:M molar ratio were also sintered at 1150°C, 1250°C, and 1350°C. In addition, YSZ-PO with a 5:1 Glucose:M molar ratio was sintered at 850°C and 950°C. In all cases, the sintered samples were black indicating that amorphous carbon had formed in situ.<sup>41</sup> Upon calcination in air at 700°C, the samples were white for YSZ and STO, yellow for GDC, and black for LSCF.

Phase identification of both the sintered and calcined materials was determined with powder X-ray diffraction (PXRD). The PXRD patterns were collected using a Bruker D2 Phaser X-ray diffractometer, with a  $2\Theta$  range of  $20^\circ\text{--}\bar{6}5^\circ,\,0.03^\circ$  increments, and 0.3 s time steps.  $CuK\alpha$  radiation was used and the stage was rotated one revolution per minute. Carbon template concentration was determined with thermogravimetric analysis (TGA) as described in our previous work.<sup>41</sup> TGA data were collected with a TA Instruments SDT Q600 by heating the sample from ambient temperature to 1200°C at a 10°C ⋅ min<sup>-1</sup> ramp rate in air flowing at 100 mL·min<sup>-1</sup>. Specific surface area was de-

Table I. Experimental summary of hybrid inorganic-organic materials preparation. Shown are reagents, molar ratios, and reaction conditions used to prepare each hybrid.

		Propylene Oxide Hybrid Materials			Citric Acid Hybrid Materials			
		YSZ	GDC	LSCF	YSZ	GDC	LSCF	STO
Reagents	Inorganic Components	$ZrCl_4 \\ Y(NO_3)_3 \cdot 6H_2O$	$CeCl_3 \cdot 7H_2O$ $GdCl_3 \cdot 6H_2O$	$\begin{array}{c} La(NO_3)_3 \cdot 6H_2O \\ Sr(NO_3)_2 \\ Co(NO_3)_2 \cdot 6H_2O \\ Fe(NO_3)_3 \cdot 9H_2O \end{array}$	ZrCl <sub>4</sub> YCl <sub>3</sub>	$\begin{array}{c} CeCl_3 \cdot 7H_2O \\ GdCl_3 \cdot 6H_2O \end{array}$	$\begin{array}{c} La(NO_3)_3 \cdot 6H_2O \\ Sr(NO_3)_2 \\ Co(NO_3)_2 \cdot 6H_2O \\ Fe(NO_3)_3 \cdot 9H_2O \end{array}$	TiCl <sub>3</sub> SrCl <sub>2</sub> · 6H <sub>2</sub> C
	Organic Components	Propylene Oxide (PO) Glucose			Citric Acid (CA) Ethylene Glycol (EG)			
	Solvents	Water	Water Ethanol (EtOH)	Water		Water		No Solvent
Molar Ratios	Metals(M):Solvent	Zr:Y:H <sub>2</sub> O 5.75:1:650	Ce:Gd:H <sub>2</sub> O:EtOH 4:1:475:475	La:Sr:Co:Fe:H <sub>2</sub> O 3:2:1:4:950	Zr:Y:H <sub>2</sub> O 5.75:1:1150	Ce:Gd:H <sub>2</sub> O 4:1:850	La:Sr:Co:Fe:H <sub>2</sub> O 3:2:1:4:1800	Sr:Ti 1:1
	PO:M	10:1						
	Glucose:M	5:1, 2.5:1, or 0:1						
	CA:EG:M			10:10:1, 5:5:1, or 1:1:1				
Temperatures	Reagents Dissolution	Ambient			Ambient		60°C	
	Hybrid Material Formation	Ambient	95°C	120°C	80°C	80°C	120°C	80°C
Hybrid Material Time of Formation		≤5 minutes	~36 hours	~12 hours	~6 hours			

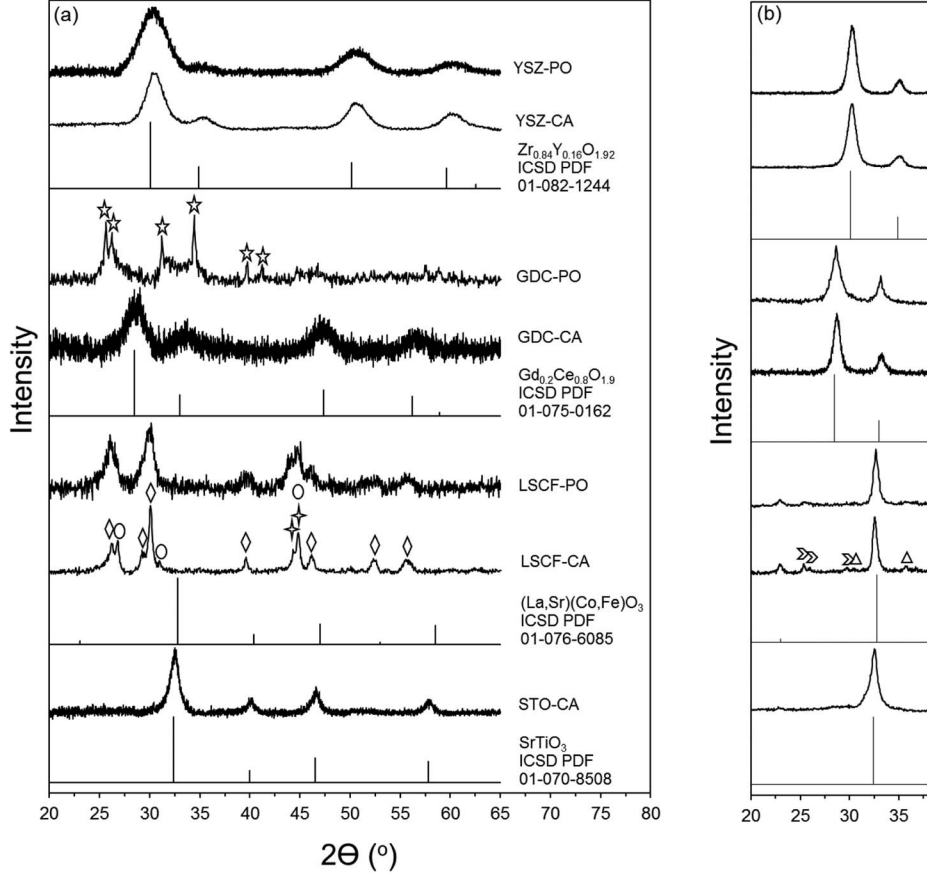
termined using the Brunauer, Emmett, and Teller (BET) method. The BET data were collected with a Micromeritics Tristar II 3020 surface area analyzer. Each sample was degassed under flowing nitrogen at 250°C for 2 h before testing. All BET experiments were conducted with nitrogen adsorption at 77 K and the correlation coefficient for all reported specific surface areas was at least 0.9995.

Symmetrical solid oxide cathode cells were fabricated by laminating three tape-casted films and sintering them in air at 1500°C. The temperature was increased from ambient temperature to 300°C, held for 3 h, then increased to 800°C, held for 3 h, then increased to 1500°C and held for 4 h, and finally decreased to ambient temperature. In all temperature ramps, a rate of 2°C ⋅ min<sup>-1</sup> was used. ESL ElectroScience YSZ (8 mol% Y<sub>2</sub>O<sub>3</sub>) film was used for the electrolyte layer and a film containing YSZ (8 mol% Y<sub>2</sub>O<sub>3</sub>, Tosoh) particles and graphite pore formers (325 mesh, Alfa Aesar) was used for both electrode layers.<sup>10</sup> The sintered cell had the following dimensions: 100 µm thick YSZ electrolyte with a cross sectional area of 1.8 cm<sup>2</sup> and symmetric 50 µm thick porous YSZ layers with a cross sectional area of 0.38 cm<sup>2</sup>. The sintered porous YSZ layers had a porosity of  $\sim$ 65%. The porous YSZ layers were infiltrated with YSZ-PO solution having a 5:1 Glucose:M molar ratio. The cell was then sintered in argon at 850°C for 2 h. The electrode layers of the sintered cells were black indicating that carbon had formed in situ inside the electrode pores. The sintered cells were then calcined in air at 700°C for 2 h to remove the carbon template. Upon calcination in air, the electrodes were white indicating complete oxidation of the carbon template. The nanostructured YSZ derived from the infiltrated YSZ-PO solution was ~2.5 vol% of the electrode. Provided that the sintered porous YSZ layers were initially ~65% porous, the nanostructured YSZ additives did not significantly affect the overall electrode porosity. The cell was subsequently infiltrated with a solution of La(NO<sub>3</sub>)<sub>3</sub> · 6H<sub>2</sub>O, Sr(NO<sub>3</sub>)<sub>2</sub>, Fe(NO<sub>3</sub>)<sub>3</sub> · 9H<sub>2</sub>O, and CA in a La:Sr:Fe:CA molar ratio of 0.8:0.2:1:2. Infiltration was repeated until a La<sub>0.8</sub>Sr<sub>0.2</sub>FeO<sub>3.8</sub> (LSF) loading of  $\sim\!25$  vol% was achieved. After each infiltration step, the cells were heated in air to 450°C. After all infiltration steps were completed, the cells were heated to 850°C for 4 h to form the LSF phase. For comparison, symmetrical LSF-YSZ cells without nanostructured YSZ were fabricated with the same procedure except for YSZ-PO solution infiltration.

Electrochemical cell performance was determined with impedance spectroscopy. A Gamry Instruments Series G750 potentiostat with four probes was used to collect the impedance spectra. Electrical contacts at both electrodes were made with Ag ink and Ag wires and all spectra were collected in the galvanostatic mode. The dc current was 0 mA, the ac perturbation was 5 mA, and the frequency ranged between  $10^5$  Hz and  $10^{-1}$  Hz. The cells with and without nanostructured YSZ were both tested in air between  $550^{\circ}\mathrm{C}$  and  $800^{\circ}\mathrm{C}$ . The non-ohmic impedances were multiplied by 0.5 to account for the contribution of two electrodes.

## Results

PXRD patterns of all the studied materials (YSZ-PO, YSZ-CA, LSCF-PO, LSCF-CA, GDC-PO, GDC-CA, and STO-CA) sintered in argon at 1050°C for 2 h are shown in Figure 2a. Patterns shown are for PO hybrid materials with a Glucose:M molar ratio of 5:1 and CA hybrid materials with a CA:EG:M molar ratio of 10:10:1. Both YSZ patterns have broad peaks matching the desired Zr<sub>0.84</sub> Y<sub>0.16</sub>O<sub>1.92</sub> standard pattern. Similarly, the STO-CA pattern peaks are broad and match the SrTiO<sub>3</sub> standard pattern. Moreover, the few prominent



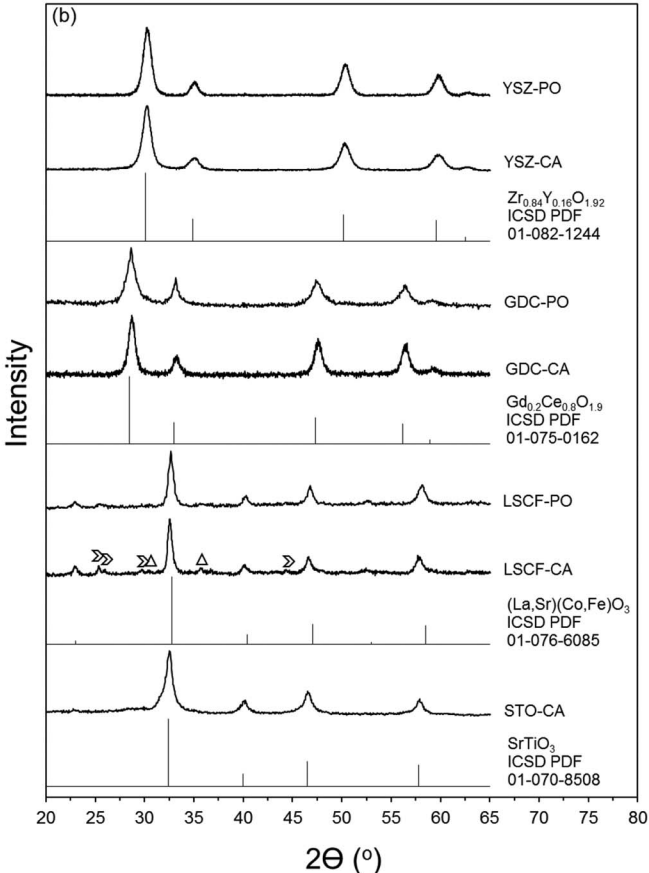


Figure 2. X-ray diffraction patterns of PO and CA hybrid materials a) sintered in argon at  $1050^{\circ}\text{C}$  for 2 h and b) subsequently calcined in air at  $700^{\circ}\text{C}$  for 2 h.  $Gd_xCe_{1-x}OCl(\overset{\bigstar}{\bowtie})$ , Hexagonal La<sub>2</sub>O<sub>3</sub>( $\overset{\bigstar}{\lozenge}$ ), Cubic La<sub>2</sub>O<sub>3</sub>( $\overset{\bigstar}{\bigcirc}$ ), Tetragonal Fe<sub>1.945</sub>C<sub>0.055</sub>( $\overset{\bigstar}{\circlearrowleft}$ ), SrCO<sub>3</sub>( $\overset{\bigstar}{\bowtie}$ ), Fe<sub>2</sub>O<sub>3</sub>( $\overset{\bigstar}{\bowtie}$ ).

peaks in the GDC-CA pattern correspond to the desired  $Gd_{0.2}Ce_{0.8}O_{1.9}$  standard pattern. The GDC-PO pattern as well as both LSCF patterns, however, show several peaks corresponding to phases other than the desired  $Gd_{0.2}Ce_{0.8}O_{2.\delta}$  and  $La_{0.6}Sr_{0.4}Co_{0.2}Fe_{0.8}O_{3.\delta}$  phases, respectively. The GDC-PO pattern shows several sharp peaks corresponding to  $Gd_xCe_{1-x}OCl$  and the LSCF patterns show a range of peaks corresponding to hexagonal  $La_2O_3$ , cubic  $La_2O_3$ , and tetragonal  $Fe_{1.945}C_{0.055}$  indicating that a mixture of lanthanum oxides and iron carbide formed during sintering. GDC prepared using the propylene oxide method is the only case where chloride was indicated in the XRD analysis and it was in the form of an oxychloride. For all other hybrid materials, it is assumed that chlorides are removed during sintering.

The absence of crystalline carbon peaks in any PXRD patterns suggests that an amorphous carbon template formed during sintering. As shown in Table I, the materials represented in Figure 2a comprise 78–85 vol% carbon. This suggests that if crystalline carbon had formed, it would have been the dominant phase in all PXRD patterns. Moreover, in all cases, the carbon templates were removed upon calcination in air at 700°C. This would not have happened if crystalline carbon was present as it oxidizes at higher temperatures (≥ 850°C).

Figure 2b shows PXRD patterns of the same materials presented in Figure 2a after being subsequently calcined in air at  $700^{\circ}$ C for 2 h. In all cases except for LSCF, the peaks correspond to the pure desired mixed-metal-oxide phases. Several small impurity peaks corresponding to SrCO<sub>3</sub> and Fe<sub>2</sub>O<sub>3</sub> were observed for LSCF. The presence of a SrCO<sub>3</sub> phase suggests that a small fraction of strontium failed to integrate into the LSCF lattice and may have reacted with CO<sub>2</sub> from the carbon template oxidation. The observed Fe<sub>2</sub>O<sub>3</sub> phase suggests that, after the iron carbide was oxidized, the temperature or diffusion length was not sufficient to integrate iron into the LSCF lattice. Although not shown here, pure LSCF phases were obtained upon calcination at  $900^{\circ}$ C in air. The important point is that the desired mixed-metal-oxides were obtained and their PXRD patterns had broad peaks, indicating that high surface area materials were prepared.

Figure 3 shows PXRD patterns of each material sintered in argon at different temperatures (1050°C–1350°C). The PXRD patterns for YSZ-PO and YSZ-CA as well as LSCF-PO and LSCF-CA were similar. Thus, only PXRD patterns of YSZ-PO and LSCF-PO are shown here.

Figure 3a shows PXRD patterns of YSZ-PO. Upon sintering at  $\leq$ 1050°C, pure YSZ phases with broad peaks were observed. For the YSZ hybrid materials sintered at 1150°C and higher, a ZrC phase formed and its intensity increased with increasing temperature while the intensity of the YSZ phase decreased. In all cases, the ZrC phase disappeared and the pure YSZ phase was obtained upon calcination in air at 700°C for 2 h.

PXRD patterns for LSCF-PO are shown in Figure 3b. At all sintering temperatures, the same behavior was observed: a mixture of La<sub>2</sub>O<sub>3</sub> and Fe<sub>1.945</sub>C<sub>0.055</sub> upon sintering and an LSCF phase with small SrCO<sub>3</sub> and Fe<sub>2</sub>O<sub>3</sub> impurity phases upon subsequent calcination in air.

PXRD patterns for GDC-PO and GDC-CA are shown in Figures 3c and 3d, respectively. Several peaks corresponding to  $Gd_xCe_{1-x}OCl$  were observed for GDC-PO upon sintering at all temperatures. However, the chloride is removed and the desired pure GDC phase was observed upon calcination in air for GDC-PO sintered between  $1050^{\circ}C$  and  $1250^{\circ}C$ . At  $1350^{\circ}C$ , a small  $Gd_2O_3$  peak was observed at a  $2\Theta$  of  $29.1^{\circ}$  suggesting that a small amount of Gd may have phase separated from Ce during sintering at  $1350^{\circ}C$ . Unlike GDC-PO, the few discernible peaks in the sintered GDC-CA PXRD patterns matched the  $Gd_{0.2}Ce_{0.8}O_{1.9}$  reference pattern and the pure desired GDC phase was obtained upon calcination at  $700^{\circ}C$  in air for 2 h.

Figure 3e shows PXRD patterns for STO-CA. Upon sintering at 1050°C, a pure STO phase with broad peaks was observed while only the peaks corresponding to the highest intensity peaks of the SrTiO<sub>3</sub> reference pattern were discernible at 1150°C. A TiC phase was observed starting at 1250°C and its intensity increased with temperature while the intensity of the STO phase decreased, becoming the minor phase at 1350°C. Upon calcination in air, the TiC disappeared and the

desired pure STO phase was obtained for STO-CA sintered at  $1050^{\circ}$ C,  $1150^{\circ}$ C, and  $1250^{\circ}$ C. At  $1350^{\circ}$ C, several impurity peaks corresponding to  $TiO_2$  were observed. Provided that the highest concentration of TiC phase was obtained at  $1350^{\circ}$ C, it is possible that a sufficient degree of separation between Sr and Ti atoms took place during sintering such that heating to  $700^{\circ}$ C was not enough thermal energy to diffuse  $TiO_2$  into the SrTiO<sub>3</sub> lattice.

Table II shows the carbon template volumetric concentrations of the PO and CA hybrid materials. In all cases, the hybrid materials were sintered at 1050°C in argon for 2 h. The carbon template concentration increased with an increase in organic content for all hybrid material formulations. This demonstrates that the carbon template concentration can be systematically controlled by adjusting the organic component to metal molar ratio. In all cases, wide carbon template concentration ranges were observed. For STO-CA, the carbon template concentration ranged between 40 vol% and 80 vol% of the mixed-metal-oxide/carbon template composite. For LSCF-CA, the concentration varied between 35 vol% and 85 vol% and for both YSZ-CA and GDC-CA, the ranges were between 50 vol% and 80 vol%. The PO hybrid materials allowed for a wider carbon template concentration range. The observed ranges for LSCF-PO, YSZ-PO, and GDC-PO were 8 vol% - 85 vol%, 10 vol% - 80 vol%, and 29 vol% - 85 vol%, respectively.

The materials represented in Table II were calcined in air at 700°C for 2 h and the BET surface areas of the resulting mixed-metal-oxides are shown in Table III. In all cases, the surface area increased with an increase in organic content and corresponding carbon template concentration. The most important point is that the results represented in Table III indicate that specific surface areas ranging between 10  $\rm m^2 \cdot g^{-1}$  and  $100~\rm m^2 \cdot g^{-1}$  were observed across all studied materials. If one assumed spherical particles of equal size, this surface area range would correspond to a particle size range of 100 nm - 10 nm.

In the case of LSCF-CA, a sharp increase in surface area was observed when the CA:EG:M molar ratio was changed from 5:5:1 to 10:10:1. One possible explanation is that the sharp increase in surface area is related to the citrate to metal ions charge ratio which increases with CA:EG:M molar ratio. As reported by Danks et al., citrate binds to metal ions forming homogeneous metal/citrate complexes. <sup>40</sup> The charge ratio of citrate to metal ions depends on the extent of CA deprotonation and bases such as  $NH_4OH$  or urea are often used to promote CA deprotonation. <sup>44,45</sup> In this study, we did not use bases and, thus, our solutions had a pH < 2. Thus, the degree of citrate/metal complex formation is likely less for 5:5:1 compared to 10:10:1, which could impact the resulting surface area. We are currently exploring the effect of increasing the pH on the final surface area for CA hybrid materials.

PO hybrid materials with a Glucose:M molar ratio of 5:1 and CA hybrid materials with a CA:EG:M molar ratio of 10:10:1 were sintered at higher temperatures (≥1050°C) and the resulting BET surface areas are shown in Figure 4. In addition, YSZ-PO with a 5:1 Glucose:M molar ratio was sintered at 850°C and 950°C in argon and the resulting specific surface areas are also shown in Figure 4. Generally, specific surface area was highest for materials sintered at 1050°C. One exception was GDC-CA and although its highest specific surface area was observed at 1150°C, the sueface areas were similar over the entire temperature range.

Specific surface areas higher than 45 m $^2 \cdot g^{-1}$  were obtained at all sintering temperatures for all studied materials except LSCF-CA and LSCF-PO. The lowest specific surface areas observed for LSCF-CA and LSCF-PO were 13 m $^2 \cdot g^{-1}$  and 16 m $^2 \cdot g^{-1}$ , respectively. For comparison, both LSCF-CA and LSCF-PO hybrid materials sintered directly in air at 1350°C had surface areas less than 0.1 m $^2 \cdot g^{-1}$ .

Figure 5 compares electrochemical impedance spectra of symmetrical cells with and without nanostructured YSZ derived from YSZ-PO. The addition of nanostructured YSZ dramatically decreased the non-ohmic impedance at  $550^{\circ}$ C and the change in impedance became less pronounced with increasing temperature. As shown in Figure 5a, the reduction in non-ohmic impedance was  $1.4~\Omega \cdot \text{cm}^2$  (45%) at  $550^{\circ}$ C,  $0.26~\Omega \cdot \text{cm}^2$  (26%) at  $600^{\circ}$ C, and  $0.075~\Omega \cdot \text{cm}^2$  (20%) at

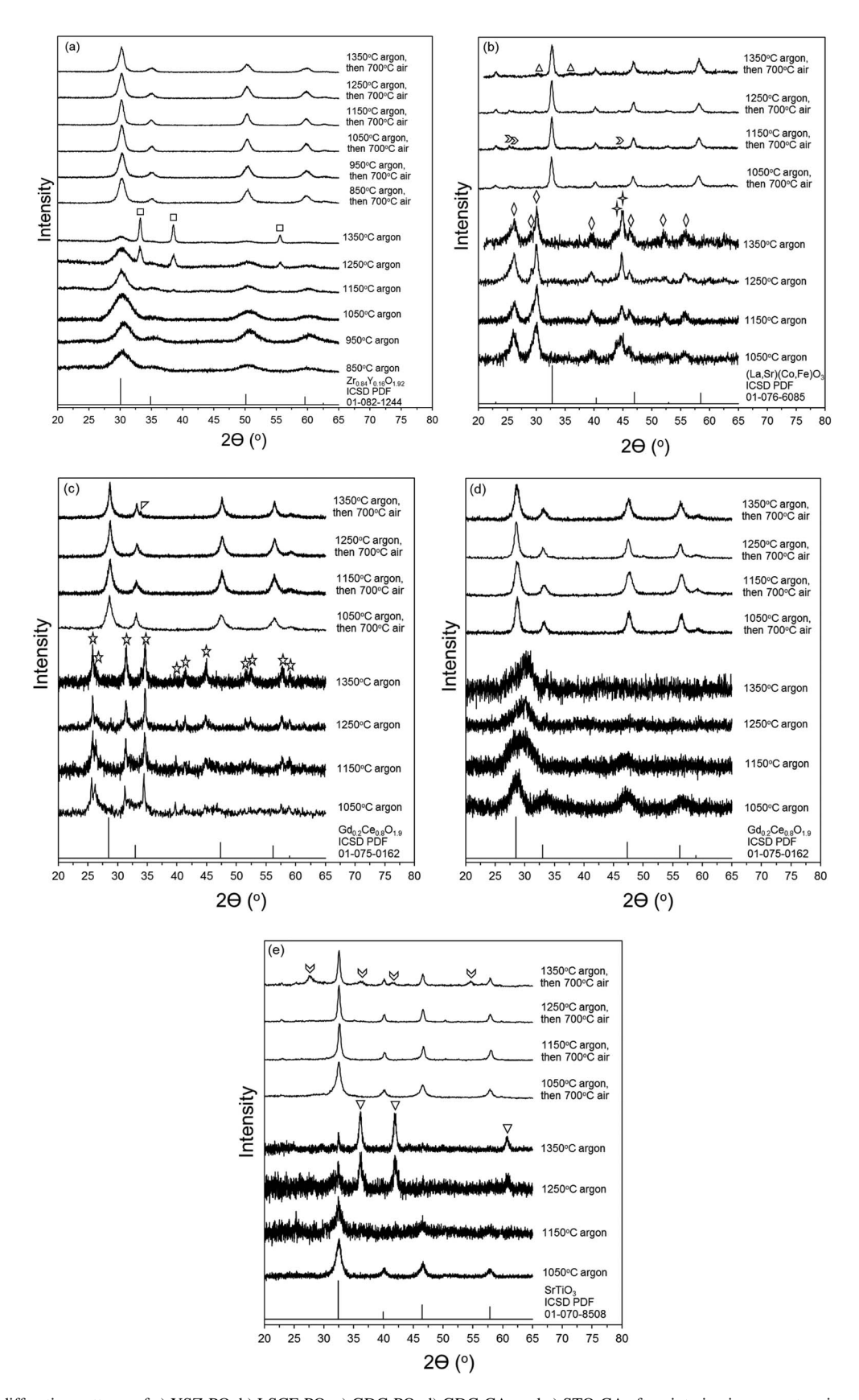


Figure 3. X-ray diffraction patterns of a) YSZ-PO, b) LSCF-PO, c) GDC-PO, d) GDC-CA, and e) STO-CA after sintering in argon at various temperatures for 2 h and after calcining in air at 700°C for 2 h. ZrC ( $\square$ ), Fe<sub>2</sub>O<sub>3</sub> ( $\triangle$ ), SrCO<sub>3</sub> ( $\triangleright$ ), La<sub>2</sub>O<sub>3</sub> ( $\stackrel{\checkmark}{\lor}$ ), Fe<sub>1.945</sub>C<sub>0.055</sub> ( $\stackrel{\checkmark}{\lor}$ ), Gd<sub>2</sub>O<sub>3</sub> ( $\stackrel{\checkmark}{\lor}$ ), Gd<sub>x</sub>Ce<sub>1-x</sub>OCl ( $\stackrel{\checkmark}{\lor}$ ), TiO<sub>2</sub> ( $\stackrel{\checkmark}{\lor}$ ), TiO<sub>2</sub> ( $\stackrel{\checkmark}{\lor}$ ), TiO<sub>3</sub> ( $\stackrel{\checkmark}{\lor}$ ), TiO<sub>4</sub> ( $\stackrel{\checkmark}{\lor}$ ), TiO<sub>5</sub> ( $\stackrel{\checkmark}{\lor}$ ), TiO<sub>7</sub> ( $\stackrel{\checkmark}{\lor}$ ), TiO<sub>8</sub> ( $\stackrel{\checkmark}{\lor}$ ), TiO<sub>8</sub> ( $\stackrel{\checkmark}{\lor}$ ), TiO<sub>9</sub> ( $\stackrel{\checkmark}{\lor$ 

Table II. Carbon template concentration as a function of hybrid material formulation. Concentration is shown as vol% of the sintered mixed-metal-oxide/carbon template composite. The hybrid materials were sintered in argon at 1050°C for 2 h.

	CA:EG:M (Citric Acid Hybrid Material)			Glucose:M (PO Hybrid Material)		
	1:1:1	5:5:1	10:10:1	0:1	2.5:1	5:1
YSZ	50	57	78	10	44	80
GDC	51	69	78	29	68	85
LSCF	34	75	85	8	72	85
STO	39	66	80			

Table III. BET specific surface area, in m<sup>2</sup> · g<sup>-1</sup>, of mixed-metal-oxides as a function of hybrid material formulation. The oxides were obtained after sintering in argon at 1050°C for 2 h, followed by calcination in air at 700°C for 2 h.

	CA:E	G:M (Citric Acid Hybrid	Glucose:M (PO Hybrid Material)			
	1:1:1	5:5:1	10:10:1	0:1	2.5:1	5:1
YSZ	36	55	83	24	46	82
GDC	33	39	61	16	75	91
LSCF	9	11	66	2.1	15	45
STO	12	65	99			

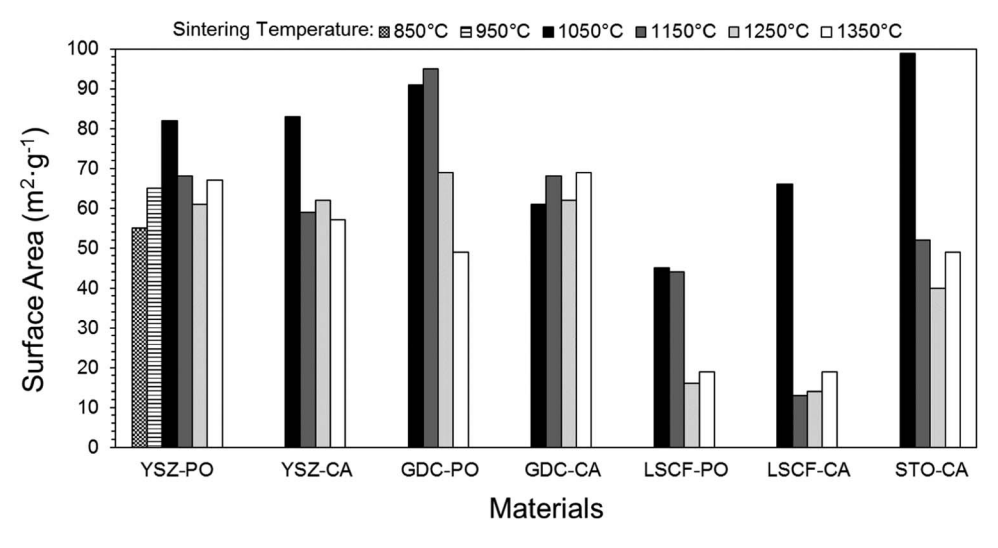


Figure 4. BET specific surface area of mixed-metal-oxides as a function of sintering temperature. The samples were sintered in argon at the indicated temperature for 2 h and then heated in air at 700°C for 2 h.

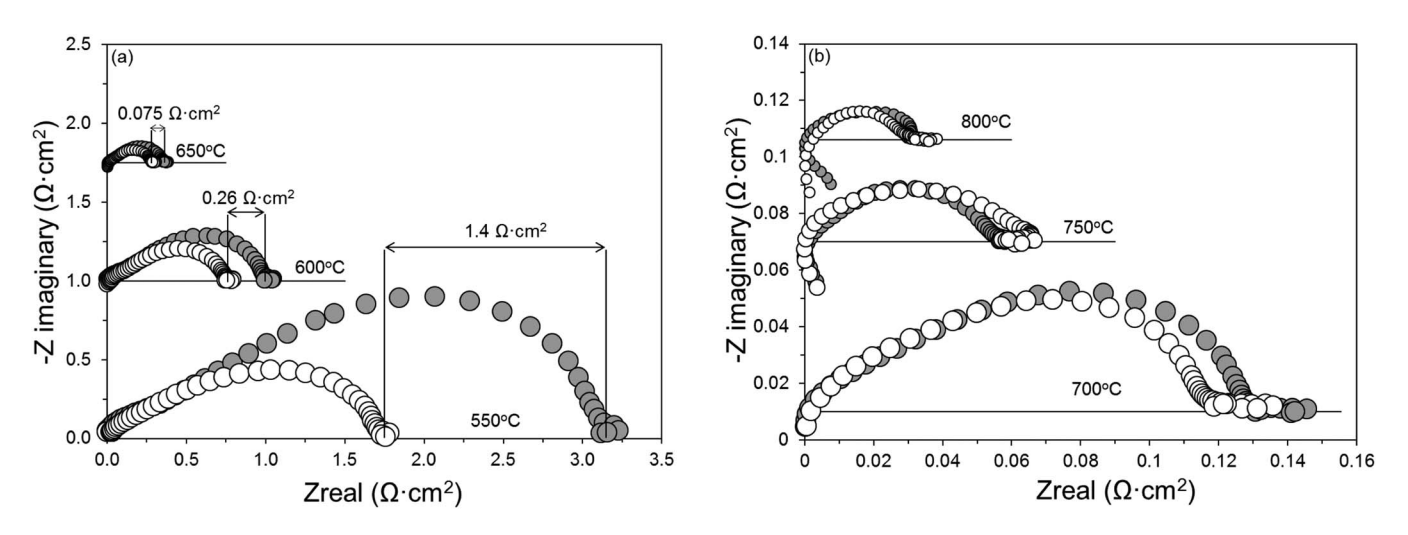


Figure 5. Electrochemical impedance spectra of LSF-YSZ symmetrical cells with traditional YSZ scaffolds ( $\bigcirc$ ) and traditional YSZ scaffolds infiltrated with YSZ-PO ( $\bigcirc$ ). After infiltration, the scaffolds were sintered in argon at 850°C for 2 h and then heated in air at 700°C for 2 h. The symmetrical cells were tested in air at a) 550°C-650°C and b) 700°C-800°C.

650°C. At 700°C the impedance decreased by 0.012  $\Omega \cdot \text{cm}^2$  (9%). Above 700°C, it was difficult to distinguish differences in impedance as shown in Figure 5b. This suggests that the electrochemical activity of LSF was sufficiently high in the 750°C–800°C range such that the nanostructured YSZ did not have a significant impact. Nevertheless, the results clearly show that incorporating the YSZ-PO intensely improved performance at lower temperatures.

#### Discussion

Although very high specific surface areas have been realized at traditional sintering temperatures with the in situ carbon templating method, it is important to recognize a potentially significant limitation: a metal carbide phase may form during sintering in argon. In particular, ZrC became the primary phase for YSZ hybrid materials upon sintering at high temperature. Subsequent calcination in air at 700°C always resulted in a pure YSZ phase; however, we have not considered what happens during the transition from ZrC to YSZ. For example, based on differences in density, one would expect a transition from ZrC to YSZ to cause a dimensional change of 17%. While this dimensional change is not relevant for the low concentration of nanostructured YSZ added to the electrodes in this study (2.6 vol%), the dimensional change could be significant for higher concentrations of nanostructured YSZ.

For STO hybrid materials, TiC became the primary phase upon sintering at high temperature. In this case a TiO<sub>2</sub> impurity metal oxide phase formed upon removal of the carbon template by oxidation in air. It is likely that the TiC phase formed large enough particles that Ti could not diffuse into the STO structure during calcination. This potential limitation is also important to consider because the impurity metal oxide phase can be deleterious to the desired electrode material functionality. For example, doped SrTiO<sub>3</sub> is used as an electronic conductor in SOFC electrodes, <sup>30–32</sup> but TiO<sub>2</sub> is an electronically insulating phase.

We are currently exploring strategies to mitigate the formation of metal carbides. One strategy is to replace the inert argon sintering atmosphere with humidified hydrogen, introducing low oxygen fugacity in the sintering atmosphere. The idea is to create a high enough oxygen fugacity that the metal carbide phase is thermodynamically unfavorable, but low enough that the carbon template is not oxidized to CO or  $CO_2$  during sintering. Preliminary findings suggest this may be a promising approach.

Given that we have established a route to realizing high surface area mixed-metal-oxides for SOFC electrodes, the next step is to explore ways to integrate these high surface area materials into SOFC electrodes to improve electrochemical performance. As a proof-of-concept, we simply infiltrated YSZ hybrid material into a traditional YSZ scaffold and showed that this intensely improved YSZ-LSF electrode performance at low temperatures. We in no way attempted to optimize this approach and only tried one hybrid material processing temperature thus far. Additional studies in this space are likely to garner further performance improvements.

There are also other approaches, beyond infiltration, by which the high surface area materials could be incorporated into cells. One approach is to directly use the high surface area materials to fabricate electrode scaffolds. To accomplish this, one could study the effects of carbon template concentration and sintering temperature. Another approach of incorporating high surface area materials is to mix the hybrid materials with traditional scaffold particles and pore formers. With this approach, the ratio of the hybrid materials to traditional scaffold particles to pore formers could be iterated.

For practical application, it is critical that the nanostructured particles are thermally stable. As a preliminary experiment in this area, we studied the thermal stability of YSZ derived from YSZ-PO. The hybrid material was sintered at  $1150^{\circ}C$ , subsequently calcined at  $700^{\circ}C$ , and then held at  $500^{\circ}C$  and  $700^{\circ}C$  in air for 2000 hours. At the end of the 2000 hours, the YSZ surface area was 65  $m^2 \cdot g^{-1}$  and 35  $m^2 \cdot g^{-1}$  for  $500^{\circ}C$  and  $700^{\circ}C$ , respectively. While we have not yet explored surface area stability when integrated into a SOFC electrode, the ther-

mal stability observed in our preliminary work is quite promising for LT-SOFC.

#### **Conclusions**

The in situ carbon templating method is a promising approach for improving the performance of LT-SOFCs. The method is robust in that it can be used to prepare a variety of high surface area SOFC materials. In addition, the carbon template concentration and specific surface area can be systematically controlled over a wide range. The integration of nanostructured YSZ derived from YSZ-PO improved electrode performance between 550°C–700°C, with a performance enhancement of 45% at 550°C.

# Acknowledgments

This work was supported by the National Science Foundation Faculty Early Career Development (CAREER) award (CMMI-1651186).

#### References

- 1. E. D. Wachsman and K. T. Lee, Science, 334, 935 (2011).
- S. Ji, I. Chang, Y. H. Lee, J. Park, J. Y. Paek, M. H. Lee, and S. W. Cha, *Nanoscale Res. Lett.*, 8, 48 (2013).
- 3. M. Mogensen and S. Skaarup, Solid State Ionics, 86-88, 1151 (1996).
- 4. B. C. H. Steele, K. M. Hori, and S. Uchino, Solid State Ionics, 135, 445 (2000).
- 5. S. M. Haile, Acta Mater., 51, 5981 (2003).
- Y. B. Kim, C-M. Hus, S. T. Connor, T. M. Gur, Y. Cui, and F. B. Prinz, J. Electrochem. Soc., 157, B1269-B1274 (2010).
- S. Ji, I. Chang, G. Y. Cho, Y. H. Lee, J. H. Shim, and S. W. Cha, *Int. J. Hydrog. Energy*, 39, 12402 (2014).
- 8. A. Egger, E. Bucher, M. Yang, and W. Sitte, Solid State Ionics, 225, 55 (2012).
- 9. M. D. Gross, J. M. Vohs, and R. J. Gorte, J. Mater. Chem., 17, 3071 (2007).
- 10. M. D. Gross, J. M. Vohs, and R. J. Gorte, J. Electrochem. Soc., 154, B694 (2007).
- 11. B. H. Smith and M. D. Gross, Electrochem. Solid-State Lett., 14 B1 (2011).
- 12. N. M. Vo and M. D. Gross, J. Electrochem. Soc., 159, B641 (2012).
- T. Z. Sholklapper, C. P. Jacobson, S. J. Visco, L. C. De Jonghe, and L. C., Fuel Cells, 8, 303 (2008).
- Z. Zhan, D. M. Bierschenk, J. S. Cronin, and S. A. Barnett, *Energy Environ. Sci.*, 4, 3951 (2011).
- 15. Y. Zhang and C. Xia, J. Power Sources, 195, 4206 (2010).
- 16. J. M. Vohs and R. J. Gorte, Adv. Mater., 21, 943 (2009).
- 17. S. P. Jiang, Mater. Sci. Eng. A, 418, 199 (2006).
- P. Blennow, J. Hjelm, T. Klemenso, A. H. Persson, S. Ramousse, and M. Mogensen, Fuel Cells, 5, 661 (2011).
- 19. Y. Huang, J. M. Vohs, and R. J. Gorte, *J. Electrochem. Soc.*, **151**, A646 (2004).
- H. He, Y. Huang, J. Regal, M. Boaro, J. M. Vohs, and R. J. Gorte, *J. Am. Ceram. Soc.*, 87, 331 (2004).
- S. Jung, C. Lu, H. He, K. Ahn, R. J. Gorte, and J. M. Vohs, *J. Power Sources*, 154, 42 (2006).
- Y. Huang, K. Ahn, J. M. Vohs, and R. J. Gorte, J. Electrochem. Soc., 151, A1592 (2004).
- A. N. Busawon, D. Sarantaridis, and A. Atkinson, *Electrochem. Solid-State Lett.*, 11, B186 (2008).
- 24. Z. Jiang, C. Xia, and F. Chen, *Electrochim. Acta*, 55, 3595 (2010).
- W. Wang, M. D. Gross, J. M. Vohs, and R. J. Gorte, J. Electrochem. Soc., 154, B439 (2007).
- M. D. Gross, J. M. Vohs, and R. J. Gorte, *Electrochem. Solid-State Lett.*, 10, B65 (2007).
- R. Kungas, F. Bidrawn, E. Mahmoud, J. M. Vohs, and R. J. Gorte, *Solid State Ionics*, 225, 146 (2012).
   D. Kennouche, Y-C. K. Chen-Wiegart, K. J. Yakal-Kremski, J. Wang, J. W. Gibbs,
- P. W. Voorhees, and S. A. Barnett, *Acta Mater.*, **103**, 204 (2016).
- J. Ju, J. Lin, Y. Wang, Y. Zhang, and C. Xia, J. Power Sources, 302, 298 (2016).
   C. D. Savaniu and J. T. S. Irvine, Solid State Ionics, 192, 491 (2011).
- A. L. Vincent, A. R. Hanifi, J-L. Luo, K. T. Chuang, A. R. Sanger, T. H. Etsell, and P. Sarkar, J. Power Sources, 215 301 (2012).
- 32. X. Shen and K. Sasaki, J. Power Sources, 320, 180 (2016).
- 33. S. Choi, S. Yoo, J-Y. Shin, and G. Kim, *J. Electrochem. Soc.*, **158**, B995 (2011).
- M. D. Gross, K. M. Carver, M. A. Deighan, A. Schenkel, B. M. Smith, and A. Z. Yee, *J. Electrochem. Soc.*, 156, B540 (2009).
- J-S. Park, I. D. Hasson, M. D. Gross, C. Chen, J. M. Vohs, and R. J. Gorte, *J. Power Sources*, 196, 7488 (2011).
- A. J. L. Reszka, R. C. Snyder, and M. D. Gross, *J. Electrochem. Soc.*, 161, F1176 (2014).
- M. J. Synodis, C. L. Porter, N. M. Vo, A. J. L. Reszka, M. D. Gross, and R. C. Snyder, J. Electrochem. Soc., 160, F1216 (2013).
- A. E. Gash, T. M. Tillotson, J. H. Satcher Jr., L. W. Hrubesh, and R. L. Simpson, J. Non-Cryst. Solids, 285, 22 (2001).

- A. E. Gash, T. M. Tilltson, J. H. Satcher Jr., J. F. Poco, L. W. Hrubesh, and R. L. Simpson, *Chem. Mater.*, 13, 999 (2001).
   A. E. Danks, S. R. Hall, and Z. Schnepp, *Mater. Horiz.*, 3, 91 (2016).
   M. Cottam, S. Muhoza, and M. D. Gross, *J. Am. Ceram. Soc.*, 99, 2625 (2016).
   S. P. Muhoza, M. A. Cottam, and M. D. Gross, *J. Vis. Exp.*, 122, e55500 (2017).

- S. P. Muhoza, T. E. Barrett, S. E. Soll, and M. D. Gross, *ECS Trans.*, 78, 1407 (2017).
   A. Chowdhury, S. O'Callaghan, T. A. Skidmore, C. James, and S. J. Milne, *J. Am. Ceram. Soc.*, 92, 758 (2009).
- 45. A. Abreu Jr, S. M. Zanetti, M. A. S. Oliveira, and G. P. Thim, J. Eur. Ceram. Soc., **25**, 743 (2005).